
Article:
Robshaw, T.J. orcid.org/0000-0002-9816-8236, James, A.M., Hammond, D.B. et al. (3 more authors) (2020) Calcium-loaded hydrophilic hypercrosslinked polymers for extremely high defluoridation capacity via multiple uptake mechanisms. Journal of Materials Chemistry A, 8 (15). pp. 7130-7144. ISSN 2050-7488

https://doi.org/10.1039/c9ta12285k

Journal of
Materials Chemistry A

Materials for energy and sustainability

Accepted Manuscript

This article can be cited before page numbers have been issued, to do this please use: T. J. Robshaw, A. M. James, J. Reynolds, D. Hammond, R. Dawson and M. Ogden, *J. Mater. Chem. A*, 2020, DOI: 10.1039/C9TA12285K.

ROYAL SOCIETY OF CHEMISTRY

rsc.li/materials-a

Calcium-loaded hydrophilic hypercrosslinked polymers for extremely high defluoridation capacity via multiple uptake mechanisms

Thomas J. Robshaw[a,b]*, Alex M. James[a], Deborah B. Hammond[a], Jake Reynolds[a], Robert Dawson[a] and Mark D. Ogden[b]

[a]Department of Chemistry, Dainton Building, University of Sheffield, UK, S3 7HF
[b]Separations and Nuclear Chemical Engineering Research, Department of Chemical and Biological Engineering, Sir Robert Hadfield Building, University of Sheffield, UK, S1 3JD
*Corresponding author: tjrobshaw1@sheffield.ac.uk

Abstract

Hydrophilic hypercrosslinked porous polymer networks were synthesised from 2,2-biphenol (HHCP1) and bisphenol A (HHCP2) monomers, which were assessed for remediation of highly fluoridated water. The networks were hydrophilic and the hypercrosslinking radically altered the acidity of protonation sites within the polymeric scaffolds. The polymers were metallated to produce novel, hybrid Ca-loaded adsorbents. The metal-loading affected the electron distribution of the quinonoid structures formed during polymerisation. HHCP1 had a greater exchange capacity (6.34 ± 0.17 mmol·g^{-1}) and adsorbed more Ca^{2+}, yet retained much of its original surface area, whereas HHCP2 was rendered non-porous upon metallation. Ca-loading included covalent interactions and formation of crystalline $CaCO_3$ (vaterite), from preferential CO_2 binding under ambient conditions. Both networks were effective defluoridating media, with Ca-loaded HHCP1 exhibiting a capacity among the highest yet reported for any extractant (267 ± 34 mg·g^{-1}). HHCP2-Ca had a lesser capacity of 96.2 ± 10 mg·g^{-1}, but faster uptake kinetics and was more effective at lower concentrations, attributed to stronger binding interactions. Crystalline CaF_2 (fluorite) was the dominant fluoride species formed, from both vaterite and covalently bound Ca. The networks could be used in a dynamic column system, extracted fluoride in the presence of multiple coexisting anions and were regenerable, with a potential pathway demonstrated for recovery of the adsorbed fluoride.

1. Introduction

Fluoride is a ubiquitous ionic species in environmental water.[1] The ingestion of small quantities (~0.05 mg·kg^{-1}·day^{-1}) is beneficial to humans, as it protects against dental decay.[2] However, chronic overexposure can lead to skeletal fluorosis, causing permanent contortion of limbs and bone weakness.[1,3] High fluoride ingestion is also linked to conditions including osteoporosis, infertility, brain damage and cancer.[4,5] The population forced to drink water exceeding the recommended maximum fluoride concentration (1.5 mg·L^{-1}) is estimated at >200 million worldwide.[4] Additionally, industries producing problematic fluoride-bearing wastewater include aluminium smelting, photovoltaic manufacturing, uranium enrichment and fertiliser production.[6-9]

Although fluoride is abundant (~625 mg·kg^{-1}) in the Earth's crust, the only commercial extraction methods are mining of fluorite (CaF_2) and recovery from phosphate rock processing.[10] The latter is converted almost exclusively to flurosilicic acid and the former used in steel-making, glass-etching, ceramics and production of HF, which is a feedstock for fine chemicals and industrially-important fluropolymers.[11] The rate of fluorite mining

View Article Online
DOI: 10.1039/C9TA12285K

(currently 5.8 kT·yr^{-1}) is increasing year-upon year.[10,12] Fluorite was awarded "critical mineral" status by The European Union in 2014.[13] Fluoride is thus ironically a scare commodity, as well as a threat to health and environment.

Removal and recovery of fluoride from aqueous waste streams, with cocontaminants, is problematic. Fluoride has high affinity towards common multivalent cations, especially Al^{3+}, so can exhibit complex aqueous speciation.[14] Precipitation techniques yield an amorphous sludge of no commercial value.[15] Membrane technologies have no potential route to recovery.[16] Fluoride is resistant to removal by commercial anion-exchange resins, being the least selective common anion for weak base and strong base anion functionality.[17,18] This can be reversed by instead loading a cation-exchanger with multivalent hard acid cations, which selectively bind fluoride via ligand-exchange.[19-21] However, in solutions of high ionic strength, leaching of the bound cations may occur, necessitating expensive chelating resins for durability.[22]

Nonetheless, many fluoride adsorbents have strategically incorporated or loaded such metals into the matrix. Example materials include alumina,[23] activated carbon[24] and chitosan.[25] These possessed capacity for fluoride higher than their unmodified equivalents, but an order of magnitude lower than a modified commercial resin (<10 mg·g^{-1} verses >180 mg·g^{-1}),[22] due to low degree of functionalisation and/or lack of porosity. The potential leaching of toxic metals into the effluent stream is also problematic for drinking water remediation.[16, 26] There remains a clear need for an economical alternative adsorbent, combining large surface area, high degree of functionalisation and selectivity.

Hypercrosslinked polymers (HCPs) are a sub-class of microporous organic materials, having high surface areas of ≤2000 m^2·g^{-1} and robust chemical and thermal stability.[27, 28] They are synthesised by Friedel-Crafts alkylation, whereby multiple aromatic rings are joined together, either by internal crosslinking, usually via chloromethyl substituents, or external, whereby a crosslinking unit (commonly dimethoxymethane) is added to the polymerisation. This creates a dense, permanently porous network with pore diameters commonly 0.5 – 1.5 nm.[27, 29] The first HCPs were derived from Davankov-type resins and these materials are still commonly reported.[30, 31] A single-step polymerisation was introduced by Li *et al.*[32] in the form of the "knitting" technique, which allows the fusing of small, electrophilic, aromatic monomers to form polymeric networks.

Many HCPs display affinity for CO_2 gas adsorption over N_2, hence being potential candidates for carbon capture and sequestration.[33] They have been applied for removal of organic pollutants[31] and for Pd and Cu catalysis.[34] However, the removal of ionic pollutants from water has been much less widely studied. This strategy has previously involved the grafting of functional groups onto the hypercrosslinked monolith. Li *et al.*[35] functionalised a Davankov HCP with sulfonate groups for uptake of heavy metals. Our research group recently reported a "knitted" HCP via Bronsted acid catalysis, also functionalised with sulfonate, for remediation of Sr and Cs.[36] Maximum theoretical uptake capacities were somewhat lower than expected, being ≤2 mmol·g^{-1} for monovalent ions. This was likely due to incomplete functionalisation, with active sites only being available in the mesopores, and the large metal ions not being able to fully access the micropores.[37] Fluoride, with its small ionic radius, may be an ideal target contaminant for a microporous matrix.

View Article Online
DOI: 10.1039/C9TA12285K

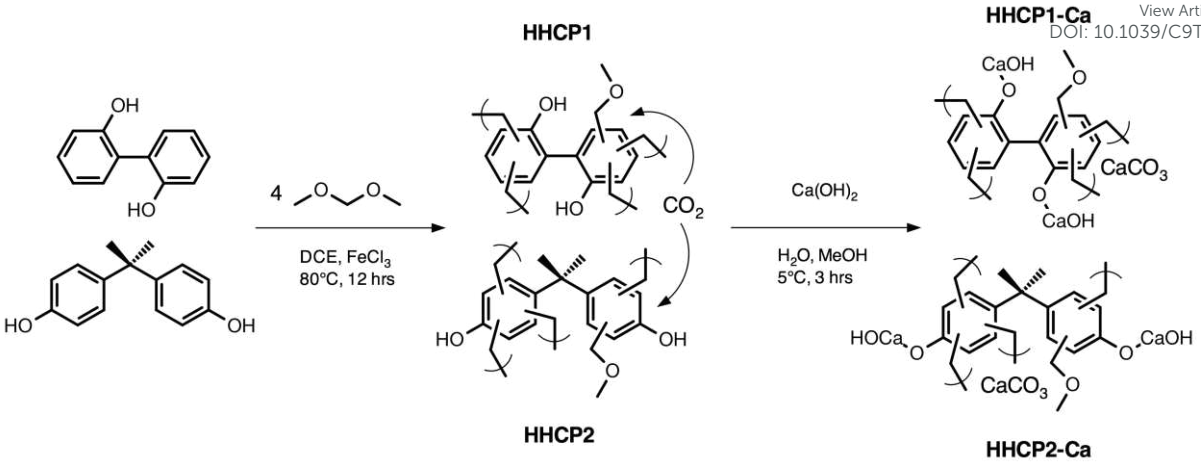

Scheme 1. Proposed synthesis of calcium-loaded hydrophilic hypercrosslinked polymers (HHCP1-Ca and HHCP2-Ca from biphenol monomers.

An alternative strategy is to embed functionality within the starting monomers, circumventing the loss of surface area observed with post-synthetic functionalisation.[35,36] This has been demonstrated in boron-rich conjugated microporous polymers (CMPs), which were selective towards fluoride adsorption, although again, with a moderate uptake capacity of 24 $mg \cdot g^{-1}$.[38] Ma *et al.* reported a porous organic framework (POF), successfully metallated, post-synthesis.[39] Both these materials however, required costly reagents for the polymerisation. In this paper, we have synergised in-built monomer functionality with strategic metal-loading with Ca to create the first metallated, hypercrosslinked polymers from two economical hydrophilic monomers 2,2'-biphenol, 4,4'-(propane-2,2-diyl)diphenol (bisphenol A) (Scheme 1). The hydrophobic monomer biphenyl, having an analogous structure to 2,2'-biphenol, is also concurrently polymerised, contacted with Ca^{2+} ions and characterised, to demonstrate the impact of hydrophilicity on the performance of the materials as defluoridating media. The potential within the strong affinity between fluoride ions and Ca-based mineral adsorbents is shown in a recent review.[40] However, the binding strength is not so great as to cause irreversible adsorption (CaF_2 $K_{sp} = 3.9 \times 10^{-11}$) and should allow facile loading/desorption cycles, since our remit is in potential recovery, as well as defluoridation. Ca^{2+} is also non-toxic and its modest ionic radius (100 pm) theoretically allows access to micropore environments and promotes a high degree of loading.

2. Methodology

2.1. Chemical reagents

All chemicals were of analytical reagent grade, unless otherwise stated, and used without further purification. For polymer synthesis, biphenyl, 2,2'-biphenol, bisphenol A and $FeCl_3$ (anhydrous) were purchased from Sigma Aldrich. 1,2-dichloroethane (DCE, anhydrous, 99 %), dimethoxymethane, $Ca(OH)_2$, and methanol were purchased from Fisher Scientific. For aqueous anion uptake experiments, Na_2CO_3, NaI, $NaNO_3$, Na_2SO_4 and KH_2PO_4 were purchased from Sigma Aldrich. NaCl and NaF were purchased from Fisher Scientific. KBr (spectroscopic grade) and NaF for fluoride analytical standards (99.999%) were purchased from Acros Organics. Deionised water (>18 mΩ) was used throughout.

2.2. Synthesis of HHCPs

View Article Online
DOI: 10.1039/C9TA12285K

In a standard synthetic procedure, a two-necked, round-bottom flask (500 mL), fitted with a stirrer, was charged with the biphenol monomer (30 mmol). This was dissolved in DCE (100 mL) and placed under nitrogen. Dimethoxymethane (10.6 mL, 120 mmol, 4 eq.) was added anhydrously, followed by a slurry of $FeCl_3$ (19.5 g, 120 mmol, 4 eq.) in the minimum quantity of DCE and the mixture was stirred at 80 °C for 12 hr. The resulting polymeric mass was washed with further DCE and methanol, then further purified by Soxhlet extraction for 12 hr. It was finally washed with HNO_3 (3 M), then NaOH (1 M), to remove as much of the trapped catalyst as possible, then deionised water until the filtrate pH was neutral, before being dried in a vacuum oven at 60 °C overnight. This afforded the final hydrophilic hypercrosslinked polymers (HHCPs) as brown powders. The 2,2'-biphenol polymer was termed HHCP1 (8.07 g, 115 %) and the bisphenol A polymer HHCP2 (9.69 g, 117 %). For the corresponding biphenyl HCP (HCP1), the same procedure was followed, with 5 eq. of crosslinker and catalyst, and resulted in a yellowy-brown powder (7.25 g, 113 %).

2.3. Calcium-loading of HHCPs

In a standard metal-loading procedure, 30 mmol of the HHCP was left in an open vial for 1 hr, to equilibrate with atmospheric gases. It was then placed in a 1:1 solution of water and methanol (2 L) in a polypropylene bottle and left to swell for 1 hr at 18 °C. $Ca(OH)_2$ (3.71 g, 50 mmol) was added and the slurry was stirred at 5 °C for 3 hr. The polymer was separated by gravity filtration and washed with water until the filtrate pH was neutral (~0.5 L). It was finally dried in a vacuum oven at 60 °C, which afforded the final product as a sepia powder (HHCP1-Ca: 11.7 g, HHCP2-Ca: 11.6 g)

2.4. Characterisation

Fourier transform infrared (FTIR) spectroscopy was performed using a Perkin-Elmer Spectrum 100. Samples were mixed with KBr (spectroscopic grade, 99.9 %) and pressed into a disk before being measured in transmission mode. Some samples were also measured using an attenuated total refraction (ATR) instrument (Perkin Elmer UATR2).

Elemental analysis (C, H and N) was performed using an Elementar Vario MICRO Cube CHN/S analyser. Cl was quantified by Schöniger oxygen flask combustion and argentometric titration. Other elements were quantified by first, acid digestion of the polymers (HNO_3/$HClO_4$), followed by appropriate dilution of the solutions and analysis via inductively-coupled plasma mass spectroscopy (ICP-MS), using an Agilent 7500CE mass spectrometer.

Scanning electron microscopy (SEM) images were recorded using an Innspect F50 field emission gun microscope, operating in secondary electron mode. Samples were mounted on carbon tape on Al stubs, without any coating treatment.

Gas sorption parameters were attained using a Micromeritics ASAP 2020Plus analyser. Nitrogen sorption measurements were analysed at -196 ºC using ~100 mg of sample. BET surface areas were calculated over a relative pressure range of 0.01-0.11 P/P_0. Error values for surface area measurements were calculated by the Micromeritics Physi ViewCalc programme via non-linear least-squares fitting. Differential pore sizes were calculated using the NLDFT method using the model for Carbon Slit Pores by NLDFT. Samples were degassed at 120 °C under dynamic vacuum immediately prior to analysis.

Solid-state NMR analysis was carried out via 1D ^{1}H-^{13}C cross-polarisation magic angle spinning (CP/MAS) experiments, using a Bruker Avance III HD spectrometer.

Powder X-ray diffraction (PXRD) spectra were attained by grinding samples in a mortar and pestle, followed by analysis using a Bruker D2 Phaser X-ray diffractometer, using a single Ni

View Article Online
DOI: 10.1039/C9TA12285K

K-β filter. Diffractograms were matched using the International Center for Diffraction Data (ICDD) PDF-4+ database.[41]

X-ray photoelectron spectroscopy (XPS) was carried out using a Kratos Supra spectrometer, with a monochromated Al source and two analysis points per sample.

Full experimental parameters are found in the Supporting Information for NMR (p12) and XPS (p18).

2.5. Determination of exchange capacities and pseudo acid dissociation constants for HHCPs

For all experiments, polymers were vacuum dried immediately prior to analysis and kept in closed containers, to prevent adsorption of CO_2. The apparent exchange capacity of HHCP1 and HHCP2 was determined, in triplicate, using Fisher-Kunin titration for weak acid cation (WAC) resins.[42] The method was unmodified, apart from no adjustment was required for degree of hydration, as the polymers were not handled in hydrated form. Pseudo stability constants were calculated by potentiometric titrations, using a modified method reported by Ogden *et al.*,[43] with a Mettler Toledo T5 Potentiometric Titrator, equipped with a standard pH electrode (DGi115-SC). A suspension of 100 mg polymer in standardized 0.00964 M HCl (50 mL) was titrated, in a closed system, against standardized 0.1008 M NaOH, with titrant additions of 0.02 mL, until the pH reached 11. Ionic strength was maintained at 1.0 M with NaCl and temperature was maintained at 18 °C, in order that neither parameter should affect H^+ activity. Titrations were completed within 2 hr and 3 repeat titrations (with pH calibration) for each polymer were acquired.

2.6. Fluoride uptake behaviour of HHCP1-Ca and HHCP2-Ca

In a typical static uptake experiment, 100 mg polymer was placed in a polypropylene vial, to which was added 25 mL of NaF solution ($[F^-]$ = 100-2000 mg·L^{-1}). The sample was sealed and placed on an orbital shaker (200 rpm) for 6 hr, until equilibrium was reached. Samples were passed through a 0.25 µm Whatman syringe filter, before being diluted appropriately for fluoride quantification. This was carried out using a Sciquip ion-selective electrode (ISE). Each sample contained 20% ionic strength adjustment buffer (preparation shown in Supporting Information, p27).

For pH-controlled experiments, samples were made up to close to final volume (22 mL), before pH adjustment was performed by addition of HCl or NaOH (0.0001-1 M). Once the desired pH was reached, samples were agitated, as previously described, for 0.5 hr, and pH was rechecked and adjusted as necessary. This process was repeated for <24 hr until equilibrium was reached, at which point, the volume was finalised and samples treated as before for analysis. For competition experiments, 25 mL of an equimolar solution of F^-, Cl^-, Br^-, I^-, NO_3^-, SO_4^{2-}, PO_4^{3-} and CO_3^{2-} (1.0 mM) was used as the contact media. Samples were diluted appropriately and analysed via anion chromatography, using a Metrohm 883 Basic IC plus, with a Metrosep A Supp 5 150/4.0 column and Na_2CO_3/$NaHCO_3$ eluent (CO_3^{2-} was not quantified, but was added to the contact solution to determine any suppression of fluoride uptake).

In a typical kinetic experiment, 2.00 g polymer was placed in 1 L polypropylene beaker, to which 500 mL NaF solution was added ($[F^-]$ = 2000 mg·L^{-1}). A timer was immediately started and small aliquots were removed from the beaker and immediately passed through a 0.25 µm Whatman syringe filter, diluted appropriately and analysed by ISE, as previously described. The total volume removed did not exceed 2 mL.

View Article Online
DOI: 10.1039/C9TA12285K

In dynamic experiments (setup shown in Figure S1), polymers were wetted with deionized water and a hydrated volume of 5.50 cm^3 was packed into a polypropylene column. This was connected to a Watson Marlow 120U peristaltic pump, using Watson Marlow Marprene® tubing, which passed an inlet NaF solution upwards through the column, with a flow rate of 2.75 $mL \cdot hr^{-1}$. The eluent was collected in polypropylene tubes, using a Bio Rad 2110 autosampler and the fractions were diluted appropriately and analysed via ISE, as before.

Two routes were attempted for regeneration of the polymer adsorbents. In the first, ~1 g fluoridated polymer was placed in a 1 L polypropylene bottle and equilibrated with 1 L NaOH (1 M) for 3 hrs. The polymer was vacuum-filtered and washed with deionized water until the filtrate pH was neutral (~0.5 L), then dried in a vacuum oven, as previously described, before repeat fluoride uptake experiments were performed. In the second method, ~1 g fluoride-loaded polymer was placed in a 1 L polypropylene bottle and equilibrated with 1 L HCl (1 M) for 3 hrs. The polymer was vacuum-filtered and washed with deionized water until the filtrate pH was neutral (~0.5 L). It was then reloaded with Ca, as previously described, before repeat fluoride uptake experiments were performed.

3. Results and discussion

3.1. Synthesis and Ca-loading of HHCPs

Both HHCPs were prepared in good yields (HHCP1: 115%, HHCP2: 117%). The generic "knitting" technique for small aromatic molecules (Scheme 1) was originally reported by Li *et al.*[32] Analogous materials to the HHCPs were first reported by Dawson *et al.,*[33] but our exact synthetic conditions were those described by James *et al.*[36] Additional acidic and alkaline washing steps, unique to this work, ensured maximal removal of any residual Fe species remaining in the networks, as these would have been likely to interact with fluoride during uptake experiments.[44] As with previous literature, yields were above the theoretical maximum, which is attributed to the presence of partially-reacted crosslinker in the final polymers.[36,45] Ca-loading was performed at 5 °C to improve $Ca(OH)_2$ solubility (Scheme 1). HHCP1-Ca and HHCP2-Ca showed significant increases in mass upon Ca-loading, as would be expected. The attempted Ca-loading of HCP1 resulted in a modest increase in mass (+ ~6%), which nonetheless suggested that some metal adsorption had occurred by an unexpected mechanism.

3.2. Characterisation

Scanning electron micrographs are shown in Figures S5-S7, which show that all networks were composed of <5 μm roughly spherical microparticles, partially fused into much larger agglomerates >10 μm in diameter. This is consistent with previous literature.[33] However, there are some interesting variations between the networks. The average size of microsphere appeared to increase in the order HCP1 > HHCP2 > HHCP. A possible explanation is that the DCE solvent can better solvate the more hydrophobic networks during the initial gelatinous polymer phase, thereby allowing the microspheres to grow larger before they fully precipitate. A similar phenomenon was reported by Cooper and Holmes.[46] The HCP1 particles were less spherical and also had a seemingly rougher surface than the biphenol polymers, which is more akin to CMPs.[47] This may imply the microstructures of HHCP1 and HHCP2 are less ordered. The SEM images did not show any obvious visual differences upon Ca-loading of the polymers. Morphological profiling may be revealing in this regard, but is beyond the scope of the present work.

Table 1 shows the composition of the networks after polymerisation and also following Ca-loading. All theoretical masses were calculated on the basis of complete crosslinking occurring at every aromatic -CH- group and exchange of both alcoholic protons in the

View Article Online
DOI: 10.1039/C9TA12285K

biphenol monomer units for a -CaOH group, which we believed was feasible.[48] HHCP1, HHCP2 and HCP1 possessed a lower C mass % than the expected theoretical figure, which is consistent with previous literature.[27,32] This has been attributed to the presence of residual $FeCl_3$ trapped in the micropores,[33] but the large discrepancies between Cl and Fe mass % suggest this is unlikely and that the Cl becomes otherwise associated during the polymerization. The unaccounted mass % can likely be attributed to extra O content, in the form of partially-reacted crosslinker,[45] or atmospheric gases adsorbed under ambient conditions.[33] For HHCP1 and HHCP2, we attempted to adjust the theoretical structure of the biphenol units within the polymer matrix, to rationalise the Ca-loading behaviour (Supporting Information, p5). From these calculations, the extent of Ca-loading was seemingly ~50% of what would be expected if every alcoholic proton was exchanged. However, as shall be seen, Ca-loading was not achieved only via covalent bonding. This does nonetheless explain why the actual C mass % in the metallated polymers was closer to the theoretical values of Table 1, because less Ca is adsorbed than expected.

Table 1. Elemental composition of the polymer networks. All elements are in units of % mass.

Network	C theoretical	C	H theoretical	H	Ca	Cl	N	Fe
HHCP1	82.1	69.3 ± 0.8	4.27	5.33 ± 0.14	<0.1	1.16 ± 0.13	1.84 ± 0.02	0.0450 ± 0.0003
HHCP2	82.6	65.8 ± 0.1	5.80	4.20 ± 0.02	<0.1	4.38 ± 0.16	<0.1	0.146 ± 0.002
HCP1	95.3	76.0 ± 0.1	4.67	4.28 ± 0.04	<0.1	8.15 ± 0.11	<0.1	0.0326 ± 0.0020
HHCP1-Ca	55.5	58.8 ± 0.4	2.89	4.92 ± 0.14	9.50 ± 0.71	0.365 ± 0.007	1.45 ± 0.01	0.0142 ± 0.0034
HHCP2-Ca	58.7	54.7 ± 0.2	4.12	3.99 ± 0.00	6.39 ± 0.46	3.46 ± 0.16	<0.1	0.1240 ± 0.0010
HCP1 + $Ca(OH)_2$	-	69.8 ± 0.7	-	4.53 ± 0.04	1.31 ± 0.08	4.97 ± 0.02	<0.1	0.0262 ± 0.0006

View Article Online
DOI: 10.1039/C9TA12285K

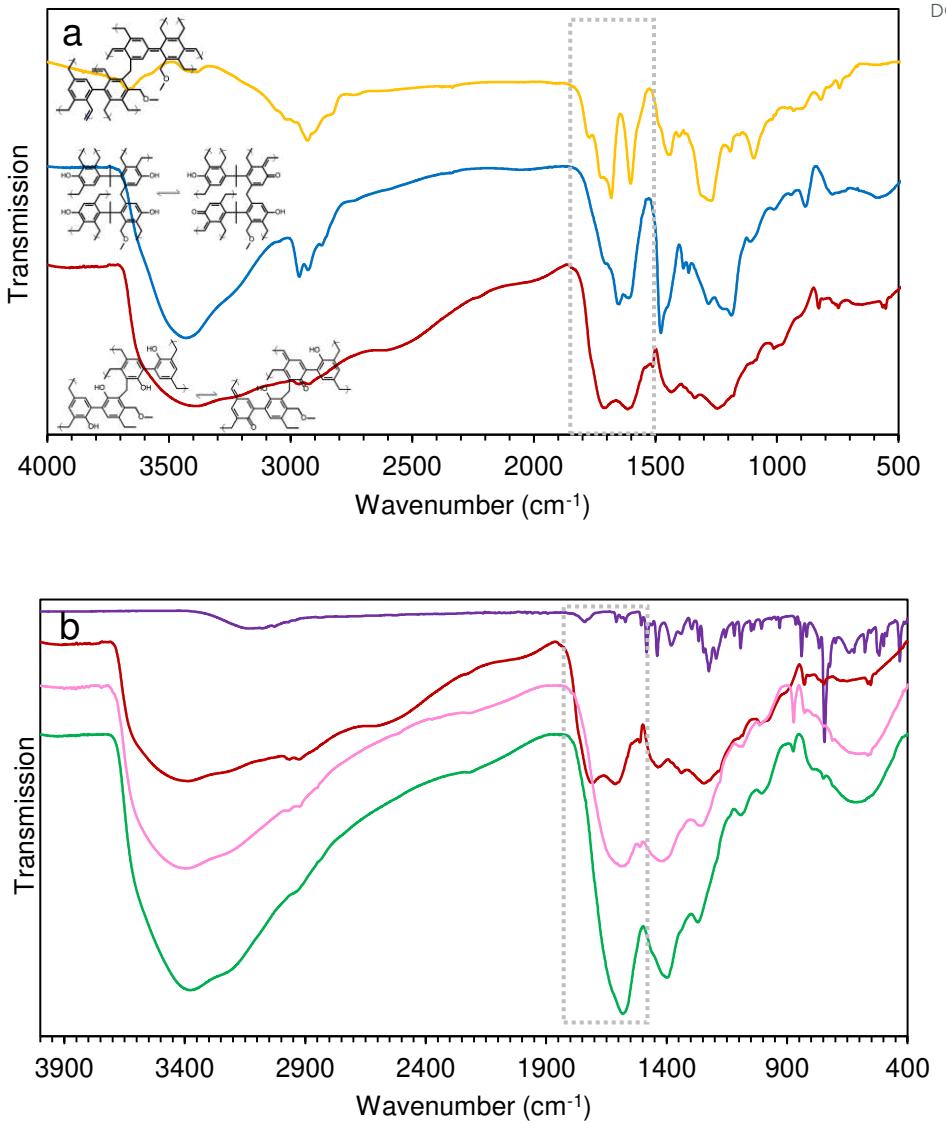

Figure 1. (a) FTIR of HHCP1 (red line), HHCP2 (blue line) and HCP1 (yellow line). **(b)** FTIR of 2,2'-biphenol monomer (purple line), HHCP1 (red line), HHCP1-Ca (pink line) and HHCP1-Ca after treatment with 500 mg·L^{-1} fluoride (green line). Quinonoid region is highlighted in each case.

In FTIR spectra, the HHCP networks exhibited broad O-H st. peaks, dissimilar to those of the parent monomers, which suggested that extensive H-bonding took place within the micropores. The HCP1 spectrum revealed the formation of quinonoid areas within the network (strong peaks ~1600-1700 cm^{-1}), due to the Hydride scavenging behaviour of $FeCl_3$, reported by Vinodh *et al.*[30] Spectra of HHCP1 and HHCP2 also showed quinonoid type peaks, but at slightly higher wavenumbers (Figure 1a and Supporting Information, p4-11), suggesting that the alcohol groups were partially incorporated into the quinonoid structures via resonance donation. In support of this, the Ca-loading of the networks seemingly altered the molecular orbital energy of the quinonoid structures, (Figure 1b) due to the phenolic oxygens now forming covalent bonds with -CaOH groups, which explains the colour change of the materials (Figures S2-S3). To confirm this theory, HHCP1 and HHCP2 were treated with 3 M NaOH, prior to FTIR analysis, to attempt to completely deprotonate the materials. This caused a striking colour change, with both networks turning black, and again, the quinonoid spectral region was altered, with a new peak appearing at ~1740 cm^{-1} (Figures S12-S13). This is predictable, since the association of alkali metal cations with phenols is an

View Article Online
DOI: 10.1039/C9TA12285K

ionic interaction (Ar-O$^-$Na$^+$), whereas the Ca interaction is a strongly polarized covalent bond (Ar-O-Ca-OH).[48] These visual and spectral changes were not observed with HCP1 (Figure S4 and S14).

The NMR spectra of HHCP1 and HHCP2 derivatives (Figure S15) supported these observations. Both spectra exhibited an intense peak at δ~120, representing cross-linked aromatic/quinonoid carbons, and a smaller peak at δ~140, representing phenolic *ipso* carbons; but also a small peak at δ160-175, which we assign to a second phenolic carbon environment, for which the bonded oxygen atom may be deprotonated with the polymer in an anhydrous state. This shifts upfield and increases with intensity upon metallation, indicating a change in the electronegativity of the oxygen. This strongly de-shielded carbon environment was not seen in spectra of the monomers (Figures S16-S17). Interestingly, there were also changes, upon metal binding, to the small peaks at δ 50-75. These likely represent the aliphatic carbons of partially-reacted crosslinkers (between an aromatic ring and a methoxy group) and could imply that these oxygen atoms also interact with metal ions.

Quantification of the differing optical properties of the networks is beyond the scope of this paper. However, these preliminary findings do indicate that optical properties of HCPs may be controlled by strategic electron-donating or withdrawing groups, which could have ramifications for their use as molecular probes, chemosensors and photovoltaic devices.[30] Figure S18 shows the possible quinonoid structures which could be adopted by HHCP1 and HHCP2 in a manner than would avoid steric hinderance of the -OH groups. It can be seen that this infers differing binding environments for the Ca^{2+} ions between the two networks, which will be discussed in due course.

XRD spectra of the non-metal-loaded networks showed the samples to be completely amorphous, as is common for MOPs.[49] However, diffractograms of HHCP1-Ca, HHCP2-Ca and HCP1 after $Ca(OH)_2$ treatment all showed peaks corresponding to crystalline $CaCO_3$ (vaterite).[41] A comparison of spectra for samples of Ca-loaded networks after contact with NaF solutions of increasing concentration (Figures S19-S20) showed the growth of CaF_2 (fluorite) peaks, with a corresponding decline in vaterite peaks, thus establishing one of the mechanisms of fluoride extraction. Both 2,2'-biphenol and bisphenol A HCPs have a proven affinity for CO_2 sorption, even with high levels of N_2 and water vapor present (isoteric heats of adsorption = 28-31 kJ·mol^{-1}).[33] However, it was unknown whether the networks were equilibrating with atmospheric CO_2 in their non-metallated forms, prior to Ca^{2+} contact, or whether the CO_2 sorption and conversion to $CaCO_3$ took place during $Ca(OH)_2$ treatment, or during exposure to the atmosphere afterwards. An experiment was conducted, described in detail in the Supporting Information (p18), which proved that the former was the case. To the best of our knowledge, the synergistic behaviour of CO_2 adsorption in ambient conditions being converted to a higher degree of functionalisation for an intended application, has not been observed previously in MOPs, although it is predictable, given their high gas adsorption capacity[50,51] and the favourability of $CaCO_3$ formation (ΔG_f^0 = -1129 kJ·mol^{-1}).

These results demonstrate that hydrophilic HCPs can be essentially activated for enhanced Ca uptake (and almost certainly other alkali earth metals) without the need for high pressure or a pure CO_2 source. It is possible that the metal-loading capacity could be enhanced still further by first exposing the polymers to, for example, a flue gas stream, which may have potential for synergistic industrial process development.

The full dataset for XPS characterisation is seen in Tables S5-S9. Figure 2a shows the wide range of C environments present in HHCP1-Ca, detectable by XPS. As expected, the most prevalent species was aromatic sp^2 carbons (284.0 eV). The peak at 285.0 eV was assigned to aliphatic crosslinkers, which had not been hydrogen-scavenged and remained sp^3-hybridised. The peak at 286.1 eV represented C-O carbons of partial crosslinkers. The 287.8

eV environment was midway between the expected binding energy of a C-O and C=O carbons respectively. This is thought to represent the *ipso* phenolic carbons and appears to confirm the partial delocalization of the π electron cloud on to the phenolic C-O bond. The most electron-poor environments were at 289.8 eV, which was characteristic of a carbonate ($CaCO_3$),[52] and at 291.6 eV, assigned to a π-π* satellite. We had no expectations of detecting adsorbed CO_2 in non-metallated samples, but surprisingly, carbonate-like environments were also observed in the spectra of HHCP1, HHCP2 and HCP1. We believe this was due to initial co-uptake of CO_2 and water vapor under ambient conditions,[33] followed by HCO_3 formation under the XPS vacuum, in a catalytically similar manner to carbonic acid formation in water.[53] The C 1s spectra of HHCP2 polymers and derivatives presented similar carbon environments, but with a higher ratio of aromatised carbons (~50%), while HCP1 samples showed an even higher proportion (~75%), indicating that quinonoid formation was more extensive in these networks. This would explain why the HCP1 SEM images were suggestive of a more ordered microstructure.

Two distinct environments were observed in the HHCP1-Ca Ca 2p spectrum (Figure 2b). The lower binding energy species (346.9 and 350.7 eV) was characteristic of $CaCO_3$.[52,54] Given the relative breadth of the peaks, it is believed that this environment also represents the polymer-bound R-O-Ca-OH species. The higher binding energy species (349.5 and 353.0 eV) is unusually electron-poor[55] and may be a result of complex formation via multiple interactions with the quinonoid pseudo-phenoxide groups, acting as neutral ligands,[56] with anionic ligands being -OH, or possibly even -Cl or -NO_3, based on elemental analysis (Table 1, Figure S25). After contact with NaF solutions, the Ca 2p spectrum shows a single environment, corresponding to a CaX_2 salt.[55] However, the breadth of the peaks could again conceal a number of similar environments. Indeed, the F 1s spectrum of HHCP1 (Figure 2c) suggests that CaF_2 (685.2 eV) is not the only species present. There are two more unusually electron-poor species present. The peak at 687.0 eV was assigned to an -RO-Ca-F group still bound to the polymer network, while the peak at 689.1 eV could represent a fluoride bridging ligand, held between two Ca centres within the micropores.[57] Electron-poor F species existing as bridging ligands in non-crystalline complexes have previously been reported from XPS probing of metal-loaded polymeric resins.[22] Ca and F environments were similar for HHCP2, but the more electron-poor Ca species was not detected (Table S8), whilst HCP1 after $Ca(OH)_2$ treatment revealed a small amount of Ca-loading had taken place, likely in the form of $CaCO_3$.

View Article Online
DOI: 10.1039/C9TA12285K

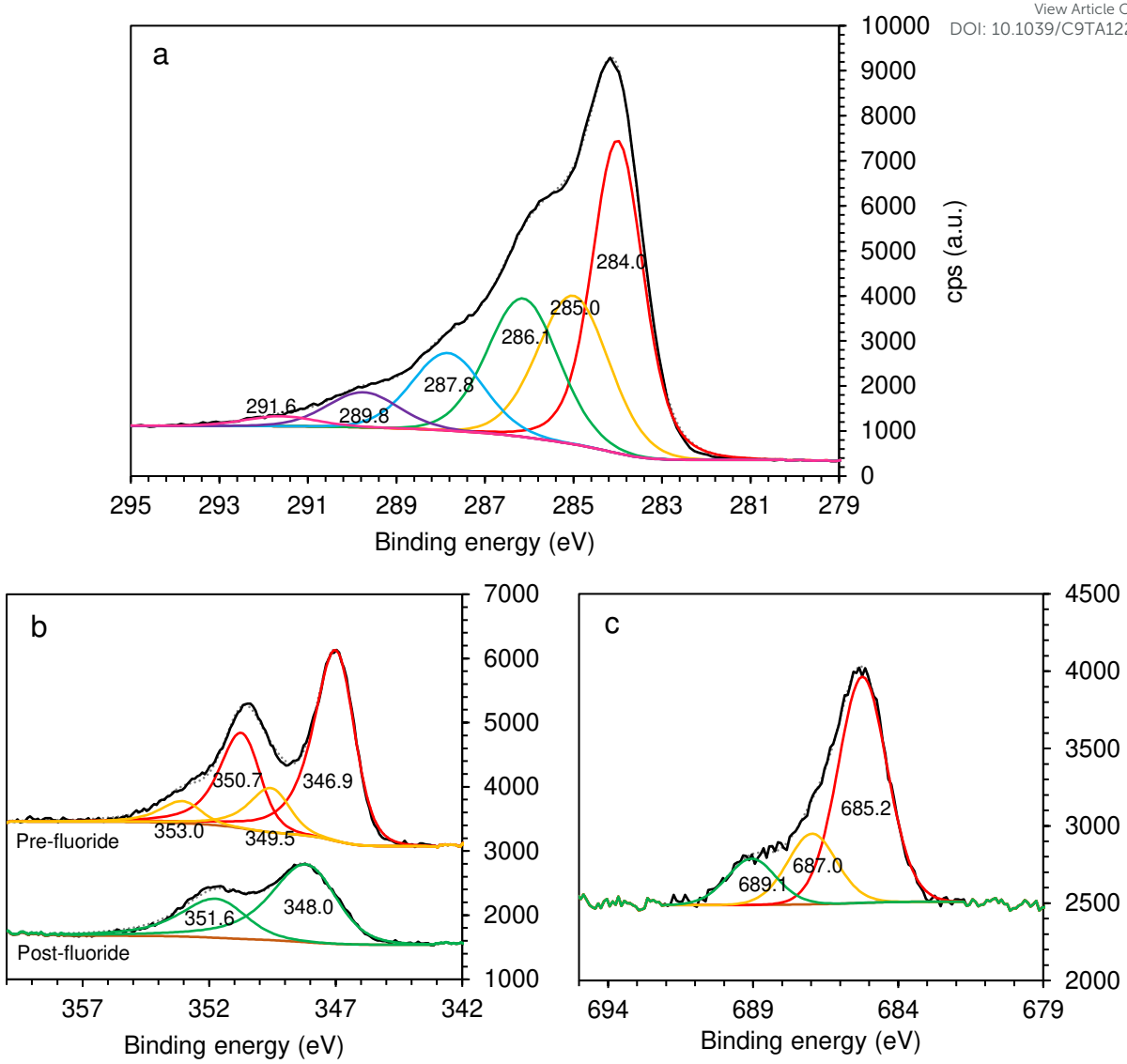

Figure 2. (a) High resolution C 1s XPS spectrum of HHCP1-Ca, with calculated peak-fitting. **(b)** High resolution Ca 2p XPS spectrum of HHCP1-Ca (top) and HHCP1-Ca after contact with 2000 mg·L^{-1} fluoride solution as NaF (bottom), with calculated peak-fitting. **(c)** High resolution F 1s XPS spectrum of HHCP1-Ca after contact with 2000 mg·L^{-1} fluoride solution as NaF.

View Article Online
DOI: 10.1039/C9TA12285K

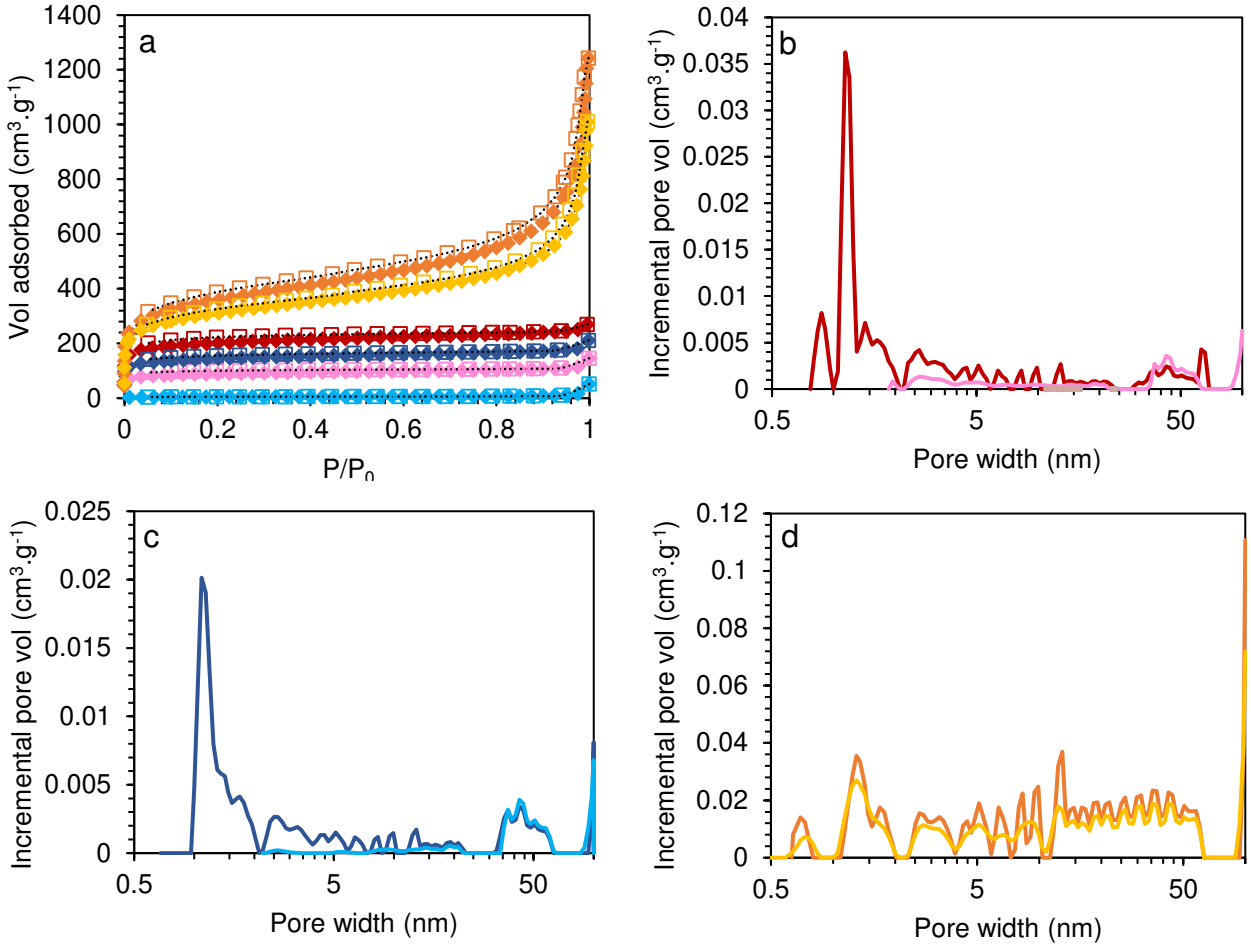

Figure 3. (a) N_2 adsorption/desorption isotherms for ◆□ HHCP1, ◆□ HHCP1-Ca, ◆□ HHCP2, ◆□ HHCP2-Ca, ◆□ HCP1 and ◆□ HCP1 after $Ca(OH)_2$ contact. Diamonds represent adsorption. Squares represent desorption. T = 77 K. **(b)** Pore size distribution, calculated by NLDFT for — HHCP1 and — HHCP1-Ca. **(c)** Pore size distribution for — HHCP2 and — HHCP2-Ca. **(d)** Pore size distribution for — HCP1 and — HCP1-Ca.

Investigation into the pore environments and surface areas of the networks, via N_2 sorption, is shown in Figure 3 and Table S10. All isotherms exhibited some type IV character, significantly so in the case of HCP1, indicating large mesopores within the samples and confirmed by pore size distribution analysis. This is common for HCP powders polymerized in a large volume of solvent, with $FeCl_3$ catalysis, as opposed to polymer monoliths.[45] HHCP1 and HCP1 had rather higher calculated surface areas than similar networks previously reported, at 748 ± 5 $m^2 \cdot g^{-1}$ and 1310 ± 1 $m^2 \cdot g^{-1}$,verses 657 $m^2 \cdot g^{-1}$ [33] and 815 $m^2 \cdot g^{-1}$.[32] HHCP2 had a slightly lesser surface area than the literature equivalent, but was still highly porous (541 ± 4 $m^2 \cdot g^{-1}$ verses 650 $m^2 \cdot g^{-1}$).[33] Such variation is common in HCP

View Article Online
DOI: 10.1039/C9TA12285K

synthesis.[32,33,36] Small adjustments in synthetic technique, such as order of addition and temperature ramping, likely effect on the prevalence of the competing reactions (crosslinking, partial crosslinking and hydrogen-scavenging). The previous high surface areas reported for these specific biphenol-based polymers was key to our selection of monomers for this study (for example, HCPs based on phenol itself are known to produce lesser surface areas of <400 $m^2 \cdot g^{-1}$,[32] so this monomer was not considered). After attempted Ca-loading, HCP1 showed a modest decrease in surface area to 1140 ± 1 $m^2 \cdot g^{-1}$, due to the $CaCO_3$ formation within the pores. However, the pore size distribution (Figure 3d) is very similar to the original polymer. HHCP1-Ca possessed a surface area of 334 $m^2 \cdot g^{-1}$, which was a more pronounced reduction, relative to HHCP1 but HHCP2-Ca had minimal micro- and mesoporosity, with a surface area of merely 17.1 $m^2 \cdot g^{-1}$. Both networks retained their larger mesopore fraction (~40 nm) upon metallation, but HHCP1-Ca also retained some smaller mesopores ~2.5 – 4 nm (Figures 3b and 3c). This may indicate that HHCP2 has narrower access channels to the mesoporous regions, which are blocked by the relatively large -CaOH groups, which may partially explain the lower Ca-loading (Table 1). Ma *et al.* reported alkali metal loading of carboxylated POFS, in which the surface area of the materials decreased according to ionic radius of the loading metal.[39] We have previously sulfonated HCPs and observed that the functionalisation took place mainly in the mesopores of the materials.[36] In this instance, the loss of surface area from Ca chemisorption is from both micropores and mesopores (Table S10), indicating that functionalisation was successful throughout the polymer matrix. Notably, HCP1, although having by far the greatest measured surface area, only achieved a small quantity of $CaCO_3$ conversion (Table 1), which demonstrates the necessity of not only porosity, but also polar group functionality in creating a suitable hydrophilic extractant for aqueous species.

3.3. Ion-exchange capacity and pseudo acid dissociation constants of HHCP1 and HHCP2

The non-metallated HHCPs were assessed for their proton uptake capacity and the apparent range of pK_a values for functional groups present in the networks (Table 2). To the best of our knowledge, these are the first such experiments carried out on microporous polymers and were intended to further probe the properties of the micropore environments created, in the context of ion-exchange behaviour. Potentiometric data were fitted, using SOLVER, to models ranging from 1-7 pK_as. (Figure 4) The experimental data for the HHCP1 network was best fit by a 4-pK_a model, while corresponding data for HHCP2 most closely agreed with a 5-pK_a model. Increasing the number of pK_as further led to inferior fitting and these results are not presented. As seen in Figure 4, a number of models gave feasible fittings to the data within experimental error and these possibilities are shown in Tables S11-S12. It should be noted that, while this technique is versatile, having been applied successfully to polymeric adsorbents,[43,58] it assumes that the molar concentrations of all different acidic groups throughout the adsorbent or ligand are equivalent, which, as has been discussed, is unlikely in these networks. However, the experiments gave an indication of the variety of acidic environments present within the polymers.

View Article Online
DOI: 10.1039/C9TA12285K

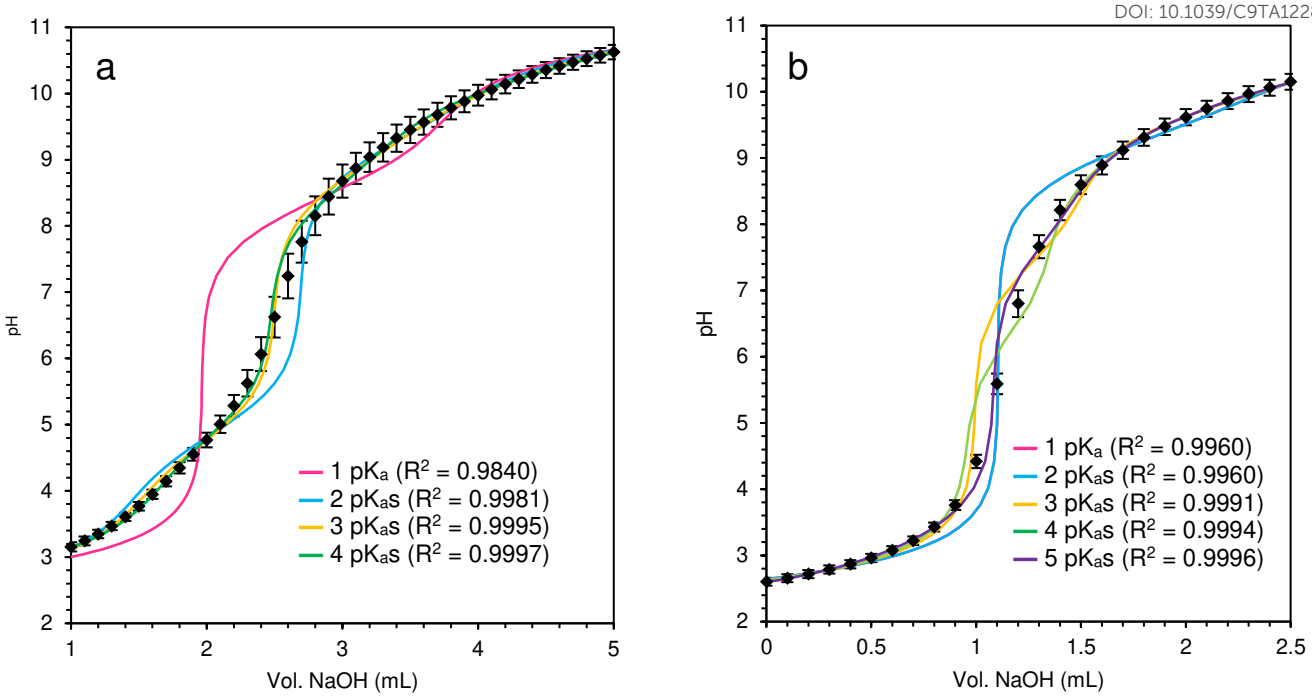

Figure 4. Potentiometic titrations of HHCP1 **(a)** and HHCP2 **(b)**, with least-squares curve-fitting to models allowing for 1 to 5 different pK_as, using Microsoft SOLVER. Error bars represent 95% confidence limits over 3 replicate titrations. T = 18°C. Ionic strength = 1.00 M. Note: for HHCP2, the 1 pK_a and 2 pK_a model lines are too close to be visually distinguished.

Table 2. Fundamental ion-exchange parameters for HHCP1 and HHCP2. Proton capacities calculated from Kunin-Fisher titration. Protonation constants from potentiometric titration, calculated from best fitting models.

Polymer	Proton capacity (mmol·g^{-1})	$Log_{10}K_1$	$Log_{10}K_2$	$Log_{10}K_3$	$Log_{10}K_4$	$Log_{10}K_5$	R^2
HHCP1	6.34 ± 0.17	10.5 ± 0.1	9.99 ± 0.06	8.48 ± 0.05	4.86 ± 0.04		0.9997
HHCP2	4.57 ± 0.25	10.1 ± 0.3	9.90 ± 0.09	9.19 ± 0.20	7.54 ± 0.12	3.33 ± 0.13	0.9996

As would be predicted from the relative masses of Ca-loading, HHCP1 had a significantly greater exchange capacity. Indeed, it is superior in this regard to even the most efficient commercial resins. The polyamine resin Purolite MTS9850 has an anion-exchange capacity of ~6.25 mmol·g^{-1} and the chelating resin Puromet MTS9501 (which has selectivity for alkali earth metals) has a reported cation-exchange capacity of only ~1.83 mmol·g^{-1}.[58,59] The capacity of HHCP2 was rather lower than expected in comparison, even given the extra mass present in the theoretical repeating unit of the polymer. This would suggest that HHCP2 featured a greater % of partial crosslinking, with the extra methoxy groups adding to the mass (Figure S8). A larger C mass % was observed in HHCP1, suggesting that the O mass % in HHCP2 may be greater (Table 1). The range of pK_as observed in both polymers was far greater than expected. Dissociation for phenolic protons typically occurs at pH ~10. However, it is known that the 2 pK_as of 2,2'-biphenol are split, with the first occurring at 7.6 (very close to the predicted $log_{10}K_4$ value for HHCP1) and the second at 13.7, due to an intramolecular hydrogen bond stabilizing the monoprotonated molecule.[60] For bisphenol A, the first pK_a is expected at 9.73,[61] but to the best of our knowledge, the second has not been reported. It is known however, that many 4,4'-biphenols also exhibit pK_a-splitting behaviour.[62] These data help to explain the pK_{1-3} values observed, as it is feasible that phenol groups of differing acidities exist within the networks, due to different extents of π cloud delocalisation, caused by quinonoid formation. The apparent pK_as below pH 5 are

View Article Online
DOI: 10.1039/C9TA12285K

more mysterious, being more suggestive of carboxylic acids. Nevertheless, they are predicted by most of the simpler models, with fewer pK_as (Tables S11-S12). It is known that hydrophobic environments, such as micropores, can lower pK_a values substantially,[43, 58] although not to the degree seen here. It is notable however, that there appear to be similar acidic functionalities present in both networks, which produce slightly lower pK_as in the HHCP2 network (10.1 vs 10.5; 9.90 and 9.19 vs 9.99; 7.54 vs 8.48), which likely has more hydrophobic pore environments, because of the alkyl bridges between phenol rings. It is also known that 3 vicinal phenol groups will form a stable $[H_2(OPh)_3]^-$ structure through H-bonding,[56] which could explain a particularly acidic proton environment (the extent of H-bonding in the networks was clear from FTIR data). Because of the probable pK_a-splitting, half of the phenolic protons in both polymers would not have dissociated under these experimental conditions.

NMR spectra (Figure S15) also support the predicted pK_as, as they suggest the existence of both protonated and deprotonated phenol groups within the polymers in an anhydrous state, having been washed to neutral pH before drying. This implies that one of the phenol groups in each monomer unit is never deprotonated or bound covalently to a metal ion. Yet the degree of deprotonation seems to be greater for the Na-loaded polymers. This is logical, as Na-loading took place using a 3 M NaOH solution, whereas the pH of the Ca-loading solution was limited by the solubility of $Ca(OH)_2$ and therefore the least acidic pK_as values for the biphenols would not be reached.[60] This explains the more pronounced colour change for the Na-loaded polymers, since greater deprotonation and ionization of the phenolic oxygens has occurred, changing the optical properties (Figures S2-S3).

Taking into account elemental analysis, XPS and titration data, the efficiency of Ca^{2+} binding by the expected covalent interactions is seemingly <50%, relative to the number of original phenol groups, with the remaining loading being in the form of $CaCO_3$. Despite the very high fluoride uptake values achieved by the existing materials, there is clearly scope for further development in terms of potentially increasing the Ca-loading still further.

3.4. Equilibrium studies for fluoride-binding to polymers under static conditions

All synthesized networks demonstrated a degree of wettability when immersed in water (Figures S27-S32), in contrast to most HCP networks.[36] The Ca-loading was beneficial to wettability, due to the increase in mass % of polar groups. The order of hydrophilicity was clearly HHCP1 > HHCP2 > HCP1, which may contribute to the differences in Ca-loading and proton capacity, and almost certainly to the acidification of pK_as.[43]

We briefly assessed the networks for their fluoride uptake capabilities by batch treatment of samples with 2000 $mg{\cdot}L^{-1}$ fluoride solutions (Figure S31). Predictably, from Ca-loading data, HHCP1-Ca and HHCP2-Ca showed large apparent equilibrium uptake capacities (q_e), at >60 $mg{\cdot}g^{-1}$, which were equal to, or greater than that observed for an Al-loaded ion-exchange resin (representative of a current industrially used adsorbent).[63] Ca-treated HCP1 had a modest uptake capacity, attributed to CaF_2 formation from the trapped $CaCO_3$ (Figure S21). HCP1 and HHCP1 also extracted a small quantity of fluoride, which may represent anion-exchange with small quantities of NO_3^- and or Cl^- trapped in the matrices. Following these data, subsequent fluoride uptake work focused solely on HHCP1-Ca and HHCP2-Ca.

We investigated the defluoridation potential of the networks over a broad pH scale and also analysed the corresponding zeta potential of the polymer surfaces (Figures S34-S35). Both networks had a wide working range, with highest fluoride q_e values observed at pH 3-7. Performance decreased at pH >7. This was a gradual decline, in the case of HHCP2-Ca and a more pronounced reduction in the case of HHCP1-Ca. Such behaviour is often attributed to competition from OH^-,[64] or to the adsorbent surface acquiring negative charge.[24] In this instance, zeta potential did not correspond exactly with fluoride uptake, as the adsorbents

are negatively charged over the whole pH range tested. This was demonstrated by linear dataplots of fluoride uptake verses zeta potential, which produced R^2 values of only 0.183 (HHCP1-Ca) and 0.0092 (HHCP2-Ca). Furthermore, at pH 8, [F^-] is still 6 orders of magnitude above [OH^-], making this explanation alone unlikely. The major uptake mechanisms may roughly be considered as the equilibria $CaCO_3 + 2\ F^- \leftrightharpoons CaF_2 + CO_3^{2-}$ and $RO\text{-}Ca\text{-}OH + 2F^- + H_2O \leftrightharpoons CaF_2 + RO\text{-}H + 2OH^-$ (XPS data suggested that the RO-Ca-F group is an intermediary, with CaF_2 formation being prevalent at higher [F^-]). CaF_2 solubility is constantly small at high pH, but increases dramatically at <3,[65,66] which coincides with the drop in defluoridation behaviour of the polymers (Figures S34-S35). The uptake of fluoride using $CaCO_3$ itself as an adsorbent also becomes gradually more unfavourable at pH >7,[66] similarly to the behaviour of HHCP2. The second equilibrium would be predicted to still be favourable ≤pH 11.5,[67] which is clearly not the case in this instance. However, a hydrophobic pore environment will modify equilibria involving salt precipitation, specifically in polymeric resins.[21,22]

There is limited correlation between defluoridation and zeta potential for both networks at higher pH, with the decrease in surface potential to <-30 mV corresponding to the almost complete loss of fluoride uptake. The zeta potential drop can be related to deprotonation of unreacted (not Ca-loaded) phenol groups which, as has been discussed, will still be present in significant quantities in HHCP1-Ca and HHCP2-Ca. According to Table 2, HHCP1-Ca deprotonation would be expected between pH 8.48 and 10.5, with HHCP2-Ca deprotonation between 9.19 and 10.1; hence the sharper increase in negative surface charge observed. The more acidic pK_as predicted by the modelling would play a lesser role in zeta potential results, as these groups would likely have been successfully converted to -CaOH active sites during metallation. We were unable to find any literature reports on the alkaline hydrolysis of calcium phenoxides or similar species. The comparatively large increase in negative surface charge between pH 8 and 10 for both networks may indeed cause electrostatic repulsion of fluoride. Hence the decreasing uptake.[24] The increasingly positive surface charge at very low pH does not equate to enhanced defluoridation, because the formation of the stable ion-pair F^-/H_3O^+ in solution.[68] Overall, both major uptake mechanisms are evidenced in the pH-dependent behaviour observed.

Because the intended remit of this work was remediation of potable water, rather than specific acidic or alkaline wastestreams, it was decided to run further experimentation at pH 7. Although HHCP2 in particular appeared to have an optimum pH range of 3-4, it was discovered that Ca^{2+} began to leach into solution at pH <3, resulting in equilibrium concentrations >50 mg·L^{-1}. Although expected (indeed, it is an indication of successful conversion of $CaCO_3$ to CaF_2),[66] this would be undesirable from a water quality point of view.

Fluoride loading isotherms were produced for both networks from initial solution concentrations of 50-2000 mg·L^{-1}. This is a larger range than is normally investigated, with most studies focussing on concentrations <50 mg·L^{-1}.[25,44,69] However, the fluoride concentration range reported in freshwater sources is similarly diverse.[70] Uptake data were fitted to four common classical adsorption models. These are presented, along with calculated parameters in the Supporting Information, p28-30.

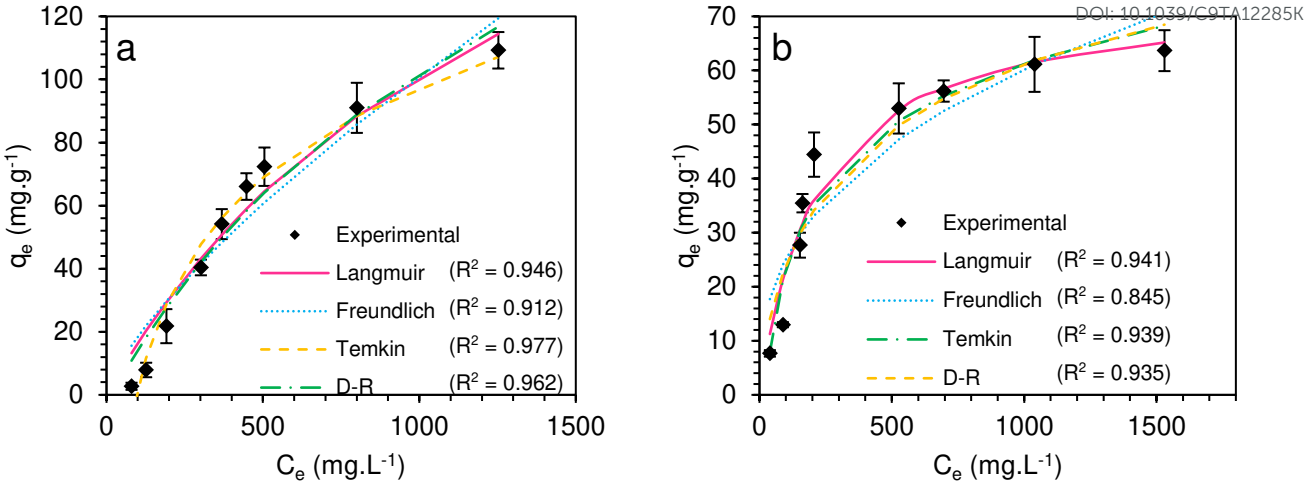

Figure 5. Fluoride loading isotherms for **(a)** HHCP1-Ca and **(b)** HHCP2-Ca (right) with two-parameter isotherm model-fitting. Error bars represent 95% confidence limits from 3 replicate samples. D-R = Dubinin-Radushkevich. C_e = equilibrium [F^-]. Polymer mass = 100 mg. Contact solution volume = 25 mL. Initial fluoride concentration = 50-2000 mg·L^{-1}. Contact time = 6 hr. T = 18°C.

Despite the similar functionalisation of the polymers, the isotherms produced were not alike (Figure 5). Both isotherms did demonstrate multilayer character, with a good description of the data given by the Temkin model. This infers that adsorption proceeds via interactions between bound and aqueous sorbate, which change in energy as a function of concentration.[71] This may reflect the different strength binding interactions between fluoride and both covalently-held Ca and $CaCO_3$. It could also be reasoned that at lower [F^-] the fluoride ions principally react with the RO-Ca-OH groups, to form the RO-Ca-F intermediate, but as [F^-] increases, the fluoride ions interact further with this adsorbed complex and crystalline CaF_2 becomes the dominant species (Table S8). This seems to happen more readily in the HHCP2 matrix, as the intermediate Ca environment was not detected by XPS. This may well be related to its greater hydrophobicity, which can be influential to the precipitation of salts on to a resin surface.[21]

Nonetheless, the isotherm for HHCP2-Ca was actually best described by the classical Langmuir model. This may be attributed to the HHCP1 polymer skeleton retaining much of its surface upon Ca-loading, allowing fluoride accumulation within the mesopores. HHCP2 in contrast, is essentially converted to a surface-functionalised medium (Figure 3) and therefore, adsorption takes the form of monolayers on the polymer particles (but still with sorbate-sorbate interactions, hence the good Temkin fitting). This would also explain the significantly lower capacity of HHCP2-Ca.

The multilayer nature of the fluoride adsorption by HHCP1-Ca is evidenced by the better fitting to the Freundlich isotherm, which empirically describes multilayer phenomena.[72] It is however noted that this model gave the poorest description of the uptake for both polymers. This in itself shows that conversion of $CaCO_3$ to CaF_2 is not the only effective mechanism, as this process in isolation is known to follow the Freundlich isotherm.[65]

A reasonable description of adsorption by both networks was given by the Dubinin-Radushkevich (D-R) model. Comparison of the calculated desorption energy (E_{des}) of fluoride binding, calculated via this isotherm, showed that the fluoride was more strongly held by HHCP2-Ca (7.81 kJ·mol^{-1} vs 5.36 kJ·mol^{-1}). These are averaged values, assuming a Gaussian energy distribution, so cannot be correlated to specific chemical interactions. They do however suggest that uptake by the HHCP1-Ca system is mainly physisorption (generally

<8 kJ·mol^{-1}), whereas the HHCP2-Ca system may be more dependent on ion-exchange or chemisorption processes (generally >8 kJ·mol^{-1}).[43,58] The E_{des} value for fluoride extraction by metal centre ligand-exchange is ~15 kJ·mol^{-1}.[22] It is not appropriate to consider an overall "binding energy" for the conversion of $CaCO_3$ to CaF_2, as it is a complex interaction, which includes adsorption, dissolution and precipitation processes.[66] However, the activation energy for CaF_2 conversion from $CaCO_3$ is rather lower than for the ligand-exchange reaction (~40 kJ·mol^{-1} vs ~60 kJ·mol^{-1}).[73,74] We therefore predict that the HHCP1-Ca system is more strongly influenced by $CaCO_3$ conversion and the HHCP2-Ca system more influenced by ligand-exchange reactions.

We monitored both the change in [OH^-] and [Ca^{2+}] in NaF solutions at various initial concentrations, after being equilibrated with HHCP1-Ca and HHCP2-Ca samples, as described previously (Figure S36). It was observed that equilibrium [OH^-] increased alongside initial [F^-], seemingly providing proof for the ligand-exchange mechanism. From the experimental data of HHCP1-Ca, considerably more OH^- was exchanged at 2000 mg·L^{-1} F^-, whereas for the HHCP2-Ca data, the difference in OH^- release between 400 mg·L^{-1} and 2000 mg·L^{-1} F^- was modest. This is concurrent with isotherm data, showing that HHCP2-Ca exchange sites become exhausted at lower [F^-]. For both polymers, the quantity of Ca^{2+} leached reduced markedly in NaF solutions, relative to deionized water. Ca^{2+} dissolution is an essential driving force for the mechanism of CaF_2 formation from $CaCO_3$,[66] but at higher [F^-], the saturation point with respect to CaF_2 is instantly reached in the particle solvation layer[73] and fluorite precipitates in areas of high local surface Ca density, principally at the edges of retreating calcite crystal terraces.[66] This presumably also in areas of high covalently-bound Ca concentration, acting as nucleation sites for CaF_2 crystals. similar phenomena have been reported for metallated ion-exchange resins.[22] The overall chemistry of the Ca-loading and fluoride uptake processes are thus elucidated and summarised in Scheme 2.

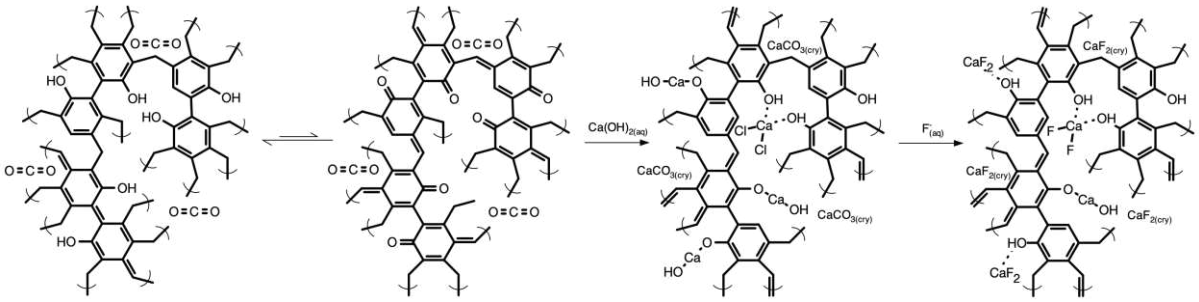

Scheme 2. Proposed Ca-loading and fluoride extraction processes of HHCPs, shown using the HHCP1 matrix as an example.

Both polymers had large maximal uptake capacities, calculated by D-R isotherm (HHCP1-Ca = 267 ± 34 mg·g^{-1}; HHCP2-Ca = 96.2 ± 10 mg·g^{-1}), which compare favourably to the literature (Table S14). As far as we are aware, only layered double hydroxide clay adsorbents, which have limited selectivity for fluoride, have recorded higher capacity than these materials (318 ± 6 mg·g^{-1}).[69] HHCP1-Ca is the superior adsorbent at high [F^-], whereas HHCP2-Ca would be more appropriate at lower [F^-].

3.5. Kinetics of fluoride-binding to HHCPs under static conditions

Kinetic data were acquired for the two networks. Similarly to equilibrium data, a number of common models were applied and relevant parameters extracted (Supporting Information, p31-35). Again, the uptake characteristics for the two networks were different (Figure 6a). For the HHCP2-Ca experiment, fluoride extraction rose sharply and quickly reached a plateau, in good agreement with the pseudo second order (PSO) model (R^2 = 0.946). This

suggested the rate of adsorption would depend on the fluoride solution concentration and number of active binding sites available on the surface of the sorbent particles. However, in the case of HHCP1-Ca, the PSO model described the adsorption data less successfully (R^2 = 0.905) and underpredicted the equilibrium uptake capacity. The fluoride uptake again increased sharply, but changed to a more gradual increase from 20-80 min (Figure S37). The Elovich model gave a superior fit (R^2 = 0.971), implying that multiple mechanisms were rate limiting at different contact stages.[58] $CaCO_3$ conversion to CaF_2 is known to be a multistep rate-limiting process.[73] The data fit to diffusion-based models (Figures S38 and S40) suggested that diffusion through the mesopores was unlikely to be rate-limiting and this is supported by other studies involving similar adsorbents.[36] The slower uptake mechanism is thus likely to be the conversion of $CaCO_3$ to CaF_2 within the mesopores.

HHCP2-Ca in particular, exhibited very rapid uptake, reaching ~50% equilibrium capacity ($t_{1/2}$) in ~0.6 min (Table S15). This is more rapid than commercial metallated ion-exchange resins (in defluoridation studies, the lowest $t_{1/2}$ value recorded was 1.8 min).[44,74] The observed rate constant is lesser than that reported for the MOF MIL-88A (2.81 x 10^{-2} vs 0.17-7.20 $g \cdot mg^{-1} \cdot min^{-1}$). However, this material had a lesser equilibrium uptake capacity of 40.4 $mg \cdot g^{-1}$.[26]

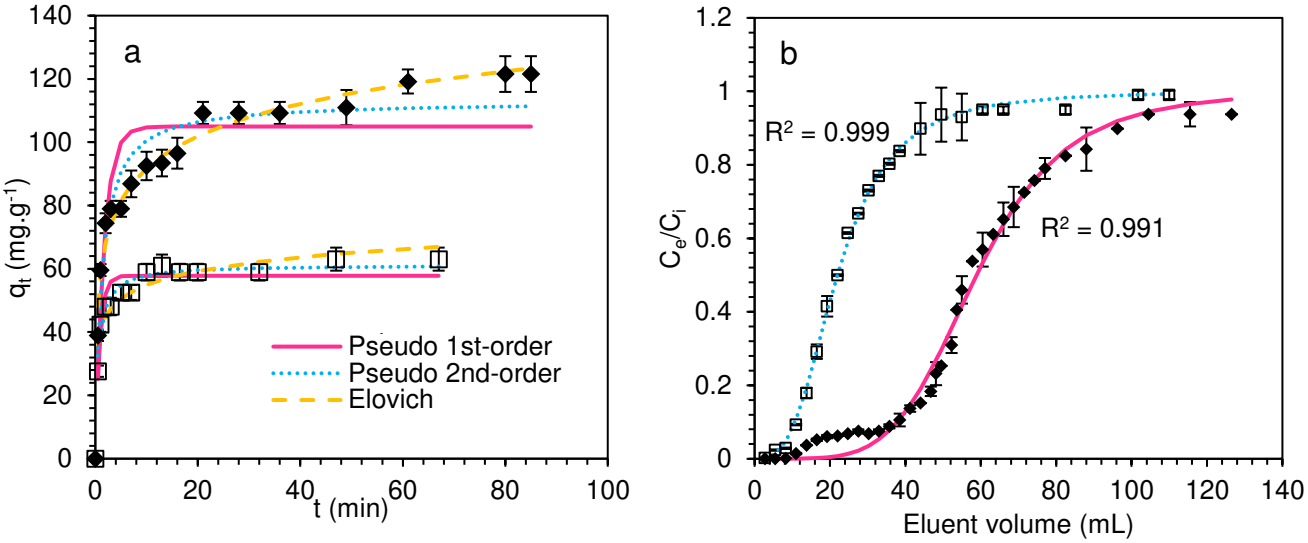

Figure 6. Static and dynamic kinetic data for the networks. **(a)** Fluoride uptake over time by HHCP1-Ca (◆) and HHCP2-Ca (□) with fitting to kinetic models. Polymer mass = 2.00 g. Contact solution initial volume = 500 mL. Initial [F^-] = 2000 $mg \cdot L^{-1}$. T = 18°C. **(b)** Dynamic fluoride breakthrough curves for HHCP1-Ca (◆) and HHCP2-Ca (□) with fitting to Dose-Response model. Inlet [F^-] = 2000 $mg \cdot L^{-1}$. T = 18°C. For both datasets, error bars represent 95% confidence limits from 3 replicate electrode measurements.

3.6. Dynamic fluoride uptake experiments, using HHCPs as ion-exchange columns

In dynamic operations, the high capacity of the polymers was again demonstrated. Data were fitted to the empirical Dose-Response model (Figure 6b),[75] which has previously successfully described fluoride breakthrough with inlet flows of high concentration.[74] This model is empirical in nature but allows calculation of a dynamic sorbent uptake capacity (Table S16). This was found to be 95.8 ± 0.8 $mg \cdot g^{-1}$ for HHCP1-Ca and 58.4 ± 0.4 $mg \cdot g^{-1}$ for HHCP2-Ca, which are close to the figures observed for static equilibrium experiments at equivalent [F^-]. It can thus be suggested that non-monolithic HCPs are suitable materials for column water treatment systems at low inlet flow rate, despite the small particle size. To the best of our knowledge, this is the first time such performance has been demonstrated.

View Article Online
DOI: 10.1039/C9TA12285K

As seen, data for HHCP1 were not perfectly modelled (Figure 6b), as the more heterogeneous adsorption resulted in a two-stage breakthrough, with a weak adsorption site of low capacity becoming exhausted before major breakthrough occurred. The main breakthrough stage was however adequately modelled. A synergistic treatment could use HHCP1-Ca (more effective at high [F^-]) as the lead column adsorbent, with HHCP2-Ca as a guard or polishing column (more effective at low [F^-]).

3.7. Polymer selectivity for fluoride ions

A successful adsorbent for fluoride remediation must also demonstrate high selectivity for the anion, in order to then elute the captured fluoride as a pure aqueous effluent, from which recovery can be attempted. In the case of contaminated groundwater, there are often positive correlations between concentrations of fluoride and other common anions (Cl^-, PO_4^{3-} and CO_3^{2-}).[70] We therefore studied competition and defluoridation-suppression effects of coexisting anions in an equimolar solution. It was observed that both polymers had high affinity for PO_4^{3-}. Indeed, the distribution coefficients (K_D) for PO_4^3 were an order of magnitude higher than for fluoride (Figures S41-S42). Surprisingly though, fluoride uptake was not suppressed by this behaviour, but enhanced, with K_D values increasing from 29.3 to 37.0 (HHCP1-Ca) and 12.3 to 19.5 (HCCP2-Ca). This was unexpected, as previous studies have reported only competitive adsorption processes for these two species.[69,76] There were no changes to the crystalline species present in samples of the networks, after contact with the mixed anions solution (Figure S23). It is possible that adsorbed PO_4^{3-} leads to the adoption of pseudo hydroxyapatite complexes within the polymer matrix, which is an effective system for defluoridation.[40,77] These experiments also revealed that Cl^- and NO_3^- were released during the uptake process. This supports the existence of a Ca species, proposed from XPS data, anchored to the network electrostatically, associated with 2 exchangeable anionic ligands. The amount of Cl^- released by HHCP2-Ca was somewhat greater (Table 1 shows there was far more Cl present in HHCP2 and HHCP2-Ca than the equivalents) and may help to explain why the desorption energy for this system was more indicative of an ion-exchange process.

3.8. Attempted regeneration of adsorbents

Several studies have used dilute NaOH to remove bound fluoride from the adsorbent.[74,78] In this instance, this treatment was only partially successful (Figure S43), due to the insolubility of the precipitated CaF_2 at high pH. The presence of unreacted fluorite within the networks after NaOH treatment was confirmed by PXRD, which also showed there was negligible $CaCO_3$ present (Figure S22). Nonetheless, both polymers retained appreciable capacity after 4 cycles of attempted NaOH regeneration, which suggests that the OH^-/F^- ligand-exchange reaction, which *is* reversible,[74] is overall the dominant uptake mechanism observed in this work. Notably, HHCP2-Ca lost more of its capacity during the NaOH cycles than HHCP1-Ca, suggesting less reversible adsorption, concurrent with the binding energies observed. In contrast, the acid regeneration process completely restored and in fact increased the performance of both polymers slightly. This may indicate that more NO_3^- anions are introduced to the material, allowing for increased defluoridation by the postulated anion-exchange mechanism. The acid regeneration route of course desorbs the Ca, as well as fluoride, from the polymers. However, this may be advantageous from an applied perspective, since the recovery of fluoride from aqueous streams, as fluorite, requires a source of Ca^{2+} in the feed.[6] It would be necessary to raise the pH of the effluent to cause fluorite precipitation, at which point, recovery should be feasible via fluidized bed treatment.[79] The two regeneration techniques could possibly be used synergistically, with NaOH treatment cycles proceeding until the performance of the polymers falls below an acceptable level, at which point, full acid-regeneration occurs and the combined effluents are pumped to the fluorite recovery stage.

View Article Online
DOI: 10.1039/C9TA12285K

4. Conclusions

We have synthesized the first metal-loaded HCPs. Porous networks derived from biphenyl, 2,2'-biphenol and bisphenol A monomers possessed high surface area and exhibited quinonoid character. Following Ca-loading of the hydrophilic systems, the HHCP1-Ca (2,2'-biphenol), surface area was still significant, owing to mesoporosity retention, but HHCP2-Ca (bisphenol A) was converted to a surface-functionalised adsorbent. The metal-loading affected the quinonoid chromophores, altering π cloud delocalisation. As well as the expected covalent binding interaction, Ca was loaded by $CaCO_3$ formation, caused by CO_2 uptake by the networks under ambient conditions. This is a new demonstration of how these already-known properties of HCPs may be capitalized on within a different remit. Non-metallated networks had proton capacities larger than for commercial ion-exchange resins and also surprisingly acidic pK_as. The cation-loading environments within the polymer pores were complex and varied, corroborated by spectroscopic techniques.

Both Ca-loaded networks possessed high defluoridation capacities, yet there were differences in loading behaviour in isotherm, kinetic and dynamic investigations. HHCP1-Ca had a greater capacity, but lower adsorption rate constants and uptake adhered more to multilayer thermodynamic models and multi-step kinetic models, due to diffusion of fluoride through the mesopores to the active sites. The dominant adsorbed species was crystalline CaF_2, formed from both $CaCO_3$ and covalently-bound Ca. Accordingly, caustic regeneration of the adsorbents was only partially successful. However, acid regeneration, followed by Ca-reloading was effective, suggesting a long potential lifespan.

Seemingly small changes in the chemistry of the polymeric matrix have wide-ranging implications for the properties of these materials as ion-exchangers. It is hoped this will stimulate further investigation into the aqueous phase interactions of microporous polymers, which may play an important role in the future management of aqueous fluoride.

Acknowledgements

The authors thank University of Sheffield associates Mr Keith Penny (Dept. Chemical and Biological Engineering), for ion chromatography technical support, Dr Cheryl Shaw (Sorby Centre), for SEM technical support and Prof Steven Armes (Dept. Chemistry), for zeta potential analysis. TJR acknowledges funding from the EPSRC (Grant no. EP/L016281/1) and Bawtry Carbon International Ltd.

References

1. M. Vithanage and P. Bhattacharya, *Environmental Chemistry Letters*, 2015, **13**, 131-147.
2. European Food Safety Authority, *Tolerable upper intake levels for vitamins and minerals*, Scientific Committee on Food, EFSA, Parma, 2006.
3. G. J. Liu, Q. F. Ye, W. Chen, Z. J. Zhao, L. Li and P. Lin, *Environmental Toxicology and Pharmacology*, 2015, **40**, 326-332.
4. A. Bhatnagar, E. Kumar and M. Sillanpää, *Chemical Engineering Journal*, 2011, **171**, 811-840.
5. World Health Organisation, *Guidelines for Drinking-water Quality. Fourth edition*, WHO Press, Geneva, 2011.
6. L. Birry, S. Leclerc and S. Poirier, *TMS (The Minerals, Metals & Materials Society)*, *Light Metals*, 2016, 467-471.
7. D. Kauspediene, R. Ragauskas, V. Pakstas and A. Gefeniene, *Chemija*, 2017, **28**, 33-38.

8. N. M. Mourad, T. Sharshar, T. Elnimr and M. A. Mousa, *Applied Radiation and Isotopes*, 2009, **67**, 1259-1268.
9. M. Potgieter, J. C. Barry, D. J. van der Westhuizen and H. M. Krieg, *Journal of the Southern African Institute of Mining and Metallurgy*, 2017, **117**, 785-792.
10. M. E. McRae, in *Mineral Commodity Surveys 2019*, ed. US Geological Survey, USGS, Reston, Virginia, 2018, pp. 60-61.
11. A. Dreveton, Manufacture of high-bulk density aluminium fluoride from fluosilicic acid (HBD-AlF_3 from FSA) and AHF, First Symposium on Innovation and Technology in the Phosphate Industry, Marrakech, 2011.
12. US Geological Survey, Mineral Commodity Summaries 2015, US Government Printing Office, Washington DC, 2015.
13. European Commission, *Communication from The Commission to The European Parliament, The Council, The European Economic and Social Committee and The Committee of The Regions. On the 2017 list of Critical Raw Materials for the EU*, European Union, Brussels, 2017.
14. U. Ntuk, S. Tait, E. T. White and K. M. Steel, *Hydrometallurgy*, 2015, **155**, 79-87.
15. P. Renuka and K. Pushpanjali, *International Journal of Engineering and Science*, 2013, **2**, 86-94.
16. K. K. Yadav, N. Gupta, V. Kumar, S. A. Khan and A. Kumar, *Environment International*, 2018, **111**, 80-108.
17. F. G. Helfferich, *Ion Exchange*, McGraw-Hill, New York, 1962.
18. S. Meenakshi and N. Viswanathan, *Journal of Colloid and Interface Science*, 2007, **308**, 438-450.
19. N. Viswanathan and S. Meenakshi, *Journal of Hazardous Materials*, 2009, **162**, 920-930.
20. I. B. Solangi, S. Memon and M. I. Bhanger, *Journal of Hazardous Materials*, 2009, **171**, 815-819.
21. G. J. Millar, S. J. Couperthwaite, D. B. Wellner, D. C. Macfarlane and S. A. Dalzell, *Journal of Water Process Engineering*, 2017, **20**, 113-122.
22. T. Robshaw, S. Tukra, D. B. Hammond, G. J. Leggett and M. D. Ogden, *Journal of Hazardous Materials*, 2019, **361**, 200-209.
23. J. M. Cheng, X. G. Meng, C. Y. Jing and J. M. Hao, *Journal of Hazardous Materials*, 2014, **278**, 343-349.
24. E. Vences-Alvarez, L. H. Velazquez-Jimenez, L. F. Chazaro-Ruiz, P. E. Diaz-Flores and J. R. Rangel-Mendez, *Journal of Colloid And Interface Science*, 2015, **455**, 194-202.
25. P. Liang, Y. Zhang, D. F. Wang, Y. Xu and L. Luo, *Journal of Rare Earths*, 2013, **31**, 817-822.
26. F. Ke, G. Luo, P. R. Chen, J. Jiang, Q. Y. Yuan, H. M. Cai, C. Y. Peng and X. C. Wan, *Journal of Porous Materials*, 2016, **23**, 1065-1073.
27. C. D. Wood, B. Tan, A. Trewin, H. J. Niu, D. Bradshaw, M. J. Rosseinsky, Y. Z. Khimyak, N. L. Campbell, R. Kirk, E. Stockel and A. I. Cooper, *Chemistry of Materials*, 2007, **19**, 2034-2048.
28. L. X. Tan and B. Tan, *Chemical Society Reviews*, 2017, **46**, 3322-3356.
29. B. Y. Li, R. N. Gong, Y. L. Luo and B. E. Tan, *Soft Matter*, 2011, **7**, 10910-10916.
30. R. Vinodh, P. Hemalatha, M. Ganesh, M. M. Peng, A. Abidov, M. Palanichamy, W. S. Chab and H. T. Jang, *RSC Advances*, 2014, **4**, 3668-3674.
31. A. M. Li, Q. X. Zhang, G. C. Zhang, J. L. Chen, Z. H. Fei and F. Q. Liu, *Chemosphere*, 2002, **47**, 981-989.
32. B. Y. Li, R. N. Gong, W. Wang, X. Huang, W. Zhang, H. M. Li, C. X. Hu and B. E. Tan, *Macromolecules*, 2011, **44**, 2410-2414.
33. R. Dawson, L. A. Stevens, T. C. Drage, C. E. Snape, M. W. Smith, D. J. Adams and A. I. Cooper, *Journal of The American Chemical Society*, 2012, **134**, 10741-10744.
34. Z. H. Guan, B. Y. Li, G. L. Hai, X. J. Yang, T. Li and B. E. Tan, *RSC Advances*, 2014, **4**, 36437-36443.

35. B. Y. Li, F. B. Su, H. K. Luo, L. Y. Liang and B. E. Tan, *Microporous and Mesoporous Materials*, 2011, **138**, 207-214.
36. A. M. James, S. Harding, T. Robshaw, N. Bramall, M. D. Ogden and R. Dawson, *Applied Materials and Interfaces*, 2019, **11**, 22464-22473.
37. J. T. M. Amphlett, M. D. Ogden, R. I. Foster, N. Syna, K. Soldenhoff and C. A. Sharrad, *Chemical Engineering Journal*, 2018, **334**, 1361-1370.
38. Z. P. Li, H. Li, H. Xia, X. S. Ding, X. L. Luo, X. M. Liu and Y. Mu, *Chemistry-A European Journal*, 2015, **21**, 17355-17362.
39. H. P. Ma, H. Ren, X. Q. Zou, S. Meng, F. X. Sun and G. S. Zhu, *Polymer Chemistry*, 2014, **5**, 144-152.
40. S. K. Nath and R. K. Dutta, *Desalination and Water Treatment*, 2015, **53**, 2070-2085.
41. T. G. Fawcett, F. Needham, C. Crowder and S. Kabekkodu, Advanced materials analysis using the powder diffraction file, 10th National Conference on X-ray Diffraction and ICDD Workshop, Shanghai, China, 2009, pp. 1-3.
42. S. Fisher and R. Kunin, *Analytical Chemistry*, 1955, **27**, 1191-1194.
43. M. D. Ogden, E. M. Moon, A. Wilson and S. E. Pepper, *Chemical Engineering Journal*, 2017, **317**, 80-89.
44. N. Viswanathan and S. Meenakshi, *Journal of Fluorine Chemistry*, 2008, **129**, 645-653.
45. C. D. Wood, B. Tan, A. Trewin, F. Su, M. J. Rosseinsky, D. Bradshaw, Y. Sun, L. Zhou and A. I. Cooper, *Advanced Materials*, 2008, **20**, 1916-1921.
46. A. I. Cooper and A. B. Holmes, Advanced Materials, 1999, 11, 1270-1274.
47. R. Dawson, A. Laybourn, R. Clowes, Y. Z. Khimyak, D. J. Adams and A. I. Cooper, Macromolecules, 2009, 42, 8809-8816.
48. R. H. Schlosberg and C. G. Scouten, *Energy & Fuels*, 1988, **2**, 582-585.
49. R. Dawson, D. J. Adams and A. I. Cooper, *Chemical Science*, 2011, **2**, 1173-1177.
50. X. Yang, M. Yu, Y. Zhao, C. Zhang, X. Y. Wang and J. X. Jiang, *RSC Advances*, 2014, **4**, 61051-61055.
51. J. Y. Lee, C. D. Wood, D. Bradshaw, M. J. Rosseinsky and A. I. Cooper, *Chemical Communications*, 2006, 2670-2672.
52. M. Ni and B. D. Ratner, *Surface Interface Analysis*, 2008, **40**, 1356-1361.
53. M. A. Henderson, *Surface Science*, 1998, **400**, 203-219.
54. F. A. Andersen and L. Brecevic, *Acta Chemica Scandinavica*, 1991, **45**, 1018-1024.
55. B. Demri and D. Muster, *Journal of Materials Processing Technology*, 1995, **55**, 311-314.
56. K. G. Caulton, M. H. Chisholm, S. R. Drake, K. Folting, J. C. Huffman and W. E. Streib, *Inorganic Chemistry*, 1993, **32**, 1970-1976.
57. S. L. Benjamin, W. Levason and G. Reid, *Chemical Society Reviews*, 2013, **42**, 1460-1499.
58. S. E. Pepper, K. R. Whittle, L. M. Harwood, J. Cowell, T. S. Lee and M. D. Ogden, *Separation Science and Technology*, 2018, **53**, 1552-1562.
59. D. N. T. Barton, T. J. Robshaw, O. Okusanya, D. Kim, S. E. Pepper, C. A. Sharrad and M. D. Ogden, *Journal of Industrial and Engineering Chemistry*, 2019, **78**, 210-221.
60. M. Jonsson, J. Lind and G. Merenyi, *Journal of Physical Chemistry A*, 2002, **106**, 4758-4762.
61. Y. H. Li, X. R. Zhai, X. S. Liu, L. Wang, H. R. Liu and H. B. Wang, *Talanta*, 2016, **148**, 362-369.
62. M. Ragnar, C. T. Lindgren and N.-O. Nilvebrant, *Journal of Wood Chemistry and Technology*, 2008, **20**, 277-305.
63. K. Oke, S. Neumann and B. Adams, *Water Today*, 2011, 76-80.
64. D. B. Bhatt, P. R. Bhatt, H. H. Prasad, K. M. Popat and P. S. Anand, *Indian Journal of Chemical Technology*, 2004, **11**, 299-303.
65. T. K. Wadhwani, *Journal of The Indian Institute of Science*, 1954, **36**, 250-258.

66. B. D. Turner, P. Binning and S. L. S. Stipp, *Environmental Science & Technology*, 2005, **39**, 9561-9568.
67. W. H. Kang, E. I. Kim and J. Y. Park, *Desalination*, 2007, **202**, 38-44.
68. P. A. Giguere and S. Turrell, *Journal of The American Chemical Society*, 1980, **102**, 5473-5477.
69. L. Lv, J. He, M. Wei, D. G. Evans and Z. L. Zhou, *Water Research*, 2007, **41**, 1534-1542.
70. S. Ali, S. K. Thakur, A. Sarkar and S. Shekhar, *Environmental Chemistry Letters*, 2016, **14**, 291-315.
71. M. Eriksson, I. Lundstrom and L. G. Ekedahl, *Journal of Applied Physics*, 1997, **82**, 3143-3146.
72. K. Y. Foo and B. H. Hameed, *Chemical Engineering Journal*, 2010, **156**, 2-10.
73. E. T. Pedrosa, L. Boeck, C. V. Putnis and A. Putnis, *American Mineralogist*, 2017, **102**, 126-134.
74. T. J. Robshaw, R. Dawson, K. Bonser and M. D. Ogden, *Chemical Engineering Journal*, 2019, **367**, 149-159.
75. G. Y. Yan, T. Viraraghavan and M. Chen, *Adsorption Science & Technology*, 2001, **19**, 25-43.
76. L. Y. Chai, Y. Y. Wang, N. Zhao, W. C. Yang and X. Y. You, *Water Research*, 2013, **47**, 4040-4049.
77. P. Gasser, Y. Haikel, J. C. Voegel and P. Gramain, *Colloids and Surfaces A-Physicochemical and Engineering Aspects*, 1994, **88**, 157-168.
78. N. Thakur, S. A. Kumar, D. N. Wagh, S. Das, A. K. Pandey, S. D. Kumar and A. V. R. Reddy, *Journal of Hazardous Materials*, 2012, **201**, 193-201.
79. R. Aldaco, A. Garea and A. Irabien, *Water Research*, 2007, **41**, 810-818.

Table of Contents Entry

View Article Online
DOI: 10.1039/C9TA12285K

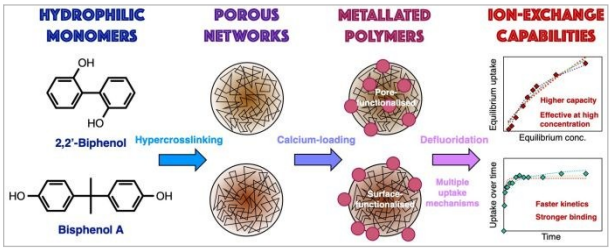

The first metallated hypercrosslinked polymers have been synthesised, characterised and found to have remarkable capacity for uptake of fluoride ions.